Available online at www.sciencedirect.com
SCIENCE DIRECT®
Journal of Solid State Chemistry 179 (2006) 195–204
JOURNAL OF SOLID STATE CHEMISTRY
www.elsevier.com/locate/jssc

Structure and magnetism of $NaRu_2O_4$ and $Na_{2.7}Ru_4O_9$

K.A. Regan[a,*], Q. Huang[b], M. Lee[c], A.P. Ramirez[d], R.J. Cava[a]

[a]Department of Chemistry, Princeton University, Princeton, NJ 08544, USA
[b]NIST Center for Neutron Research, National Institute of Standards and Technology, Gaithersburg, MD 20899, USA
[c]Department of Physics, Princeton University, Princeton, NJ 08544, USA
[d]Bell Laboratories, Lucent Technologies, Murray Hill, NJ 07974, USA

Received 4 August 2005; received in revised form 10 October 2005; accepted 16 October 2005
Available online 28 November 2005

Abstract

The structures of $NaRu_2O_4$ and $Na_{2.7}Ru_4O_9$ are refined using neutron diffraction. $NaRu_2O_4$ is a stoichiometric compound consisting of double chains of edge sharing RuO_6 octahedra. $Na_{2.7}Ru_4O_9$ is a non-stoichiometric compound with partial occupancy of the Na sublattice. The structure is a mixture of single, double and triple chains of edge-shared RuO_6 octahedra. $NaRu_2O_4$ displays temperature independent paramagnetism with $\chi_0 = 1.23 \times 10^{-4}$ emu/mol$_{Ru}$ Oe. $Na_{2.7}Ru_4O_9$ is paramagnetic, $\chi_0 = 2.0 \times 10^{-4}$ emu/mol Oe with $\Theta_w = -11.8$ K and a Curie constant of 0.0119 emu/mol Oe K. Specific heat measurements reveal a small upturn at low temperatures, similar to the upturn observed in $La_4Ru_6O_{19}$. The electronic contribution to the specific heat (γ) for $Na_{2.7}Ru_4O_9$ was determined to be15 mJ/mole$_{Ru}$ K^2.
© 2005 Elsevier Inc. All rights reserved.

Keywords: Ruthenate; Bronze; $NaRu_2O_4$; $Na_{2.7}Ru_4O_9$; Ferrite; Paramagnetic

1. Introduction

Perovskite-based alkaline earth ruthenates ($M_{n+1}Ru_nO_{2n+1}$ where M = Ca, Sr, Ba) exhibit properties ranging from ferromagnetism in $SrRuO_3$ [1], to weakly temperature-dependent paramagnetism in $BaRuO_3$ [2] and superconductivity in Sr_2RuO_4 [3]. A substantial body of research has been done on ruthenium-based perovskites to elucidate what gives rise to such a variety of magnetic behavior. The evidence suggests that ruthenates routinely border between different competing magnetic states, with subtle structural or chemical features tipping the compounds toward one behavior over another.

The extensive studies on perovskites have sparked interest in other structural families. Some have gone as far to say that the pyrochlore family offers a "potential panacea for the frustrated perovskite chemist" [4]. Unfortunately, the ruthenium-based pyrochlores do not exhibit the same broad range of magnetic behavior. Recent work on the hollandites, KRu_4O_8 and $RbRu_4O_8$, revealed temperature independent paramagnetism [5] and metallic conductivity. Although the magnetic properties of these two compounds are ordinary, hollandite $BaRu_6O_{12}$ exhibits a 1D to 3D crossover in its electrical properties at low temperatures. Some proposals have suggested that this can be explained by a quantum phase transition [6]. Further investigation of ruthenates in other structural families appears warranted, as more unusual properties may be exposed.

The Na–Ru–O system, for example, has not been thoroughly investigated, with several previously reported phases only superficially characterized [7]. Recently, Darriet et al. reported the structure and the magnetic properties of $NaRuO_2$ as well as Na_2RuO_4 [8,9]. $NaRuO_2$, a layered compound with the α-$NaFeO_2$ structure (isostructural with $NaCoO_2$, which upon deintercalation and hydration can be made superconducting [10]) displays paramagnetic behavior. Semiconducting Na_2RuO_4 adopts a new structure type, 1D in character, and is comprised of chains of corner sharing RuO_5 trigonal bipyrimids. Antiferromagnetic behavior attributed to short-range ordering is observed in this compound. The discovery of new structure types and the presence of a variety of

*Corresponding author. Fax: +1 609 258 6746.
E-mail address: kregan@princeton.edu (K.A. Regan).

0022-4596/$ - see front matter © 2005 Elsevier Inc. All rights reserved.
doi:10.1016/j.jssc.2005.10.016

magnetic and electrical properties in sodium ruthenates encourages a more through investigation of other compounds in this chemical system.

$NaRu_2O_4$ and $Na_{3-x}Ru_4O_9$ are two compounds whose structure and properties have not been well characterized. $NaRu_2O_4$ (and $NaRuFeO_4$) was first reported by Darriet and Vidal [11]. Characterization suggested temperature independent paramagnetism as well as metallic conductivity; however, no numerical data were reported for either property. Single crystal X-ray data was used to refine the structure of $Na_{3-x}Ru_4O_9$ [12]. However, four different Na contents ($x = 1$, 0.9, 0.8 and 0.25) and fractional occupations for the three Na sites were suggested, and all four models gave identical goodness of fit parameters. More recently, this compound has been investigated as an ion conductor [13]. The non-stoichiometric Na content allows for Na^+ migration within the channels at temperatures above 390 K and between the channels above 560 K. Cao et al. reported magnetic susceptiblility data and resistivity on single crystals of "$Na_2Ru_4O_{9-\delta}$" [14]. This study revealed a large anisotropy in both the resistivity and the susceptibility in a crystal believed to be oxygen deficient.

The structural similarity of both compounds to hollandite and the possibility of quasi-one dimensional behavior in $Na_{3-x}Ru_4O_9$ inspired this study. Recent work on $NaRh_2O_4$, which is isostructural with $NaRu_2O_4$ shows unconventional magnetism with Ca doping, and its resistivity changes dramatically within the solid solution [15]. Here we report the structural refinements by powder neutron diffraction patterns for both $NaRu_2O_4$ and $Na_{3-x}Ru_4O_9$, with the exact stoichiometry of $Na_{3-x}Ru_4O_9$ determined as $x = 0.3$. Magnetic susceptibility measurements were taken between 5 and 250 K. Specific heat data were collected at low temperature.

2. Experimental

Polycrystalline samples of $NaRu_2O_4$ and $Na_{2.7}Ru_4O_9$ were synthesized using Na_2CO_3 (Alfa Aesar 99.5%) and RuO_2 powder (Alfa Aesar, Ru 54% min). Both the RuO_2 powder and the Na_2CO_3 powder were heated prior to sample preparation to remove absorbed water. RuO_2 powder was heated at 700 °C for 2 h; Na_2CO_3 powder was heated at 250 °C overnight. For the synthesis of $NaRu_2O_4$, a 1:2 ratio of Na:Ru was used; a 3:4 ratio of Na:Ru was used for the synthesis of $Na_{2.7}Ru_4O_9$. The reaction mixtures were ground intimately and pressed into 1.5 cm diameter pellets. The pellets were placed together in a dense alumina boat and heated under flowing argon at 700 °C for 24 h, 850 °C for 18 h and 900 °C for 24 h. Additional heating at 900 °C was sometimes necessary to obtain $NaRu_2O_4$ as a single phase. Attempts to alter the Na content in $Na_{2.7}Ru_4O_9$ either by direct synthesis or by deintercalation using saturated I_2 solution suggested that the Na content in this phase is not variable. Attempts to prepare oxygen-deficient $Na_{2.7}Ru_4O_9$, by heating as-made powder in an evacuated quartz tube, or by other methods, caused the sample to decompose, suggesting that no significant variation of oxygen content is possible, in disagreement with a previous report [14].

Phase purity was determined via powder X-ray diffraction using Cu$K\alpha$ radiation. Resulting patterns corresponded with previously reported peak positions [11,12]. Magnetic characterization was performed at 1 T using a Quantum Design SQUID magnetometer from 5 to 250 K. The specific heat ($C(T)$) data for $Na_{2.7}Ru_4O_9$ were obtained using the relaxation method with a Quantum Design calorimeter system. The sample powder was cold-sintered into a hard disk with Ag powder (at a mass ratio of 1:1) to enhance themalization. The Ag contribution to $C(T)$ was measured separately and subtracted from the data on the composite disk. The neutron powder diffraction intensity data of both compounds were collected at the NIST Center for Neutron Research on a high-resolution powder neutron diffractometer, with monochromatic neutrons of wavelength 1.5403 Å produced by a Cu(311) monochromator. Collimators with horizontal divergences of 15′, 20′ and 7′ of arc were used before and after the monochromator, and after the sample, respectively. Data were collected in the 2θ range of 3° and 168°, with a step size of 0.05′. The structural parameters were refined using the program GSAS [16]. The neutron scattering amplitudes used in the refinement were 0.363, 0.721, and 0.581 ($\times 10^{-12}$ cm) for Na, Ru and O, respectively.

3. Results

3.1. Structure

The structure of $NaRu_2O_4$ was refined in the orthorhombic space group *Pnma* (#62) with lattice parameters of $a = 9.2737(4)$ Å, $b = 2.8215(1)$ Å, and $c = 11.1701(5)$ Å. The calcium ferrite structure ($CaFe_2O_4$) was used as an initial structural model. The refinement results are in good agreement with a previous refinement done using X-ray diffraction data [11]. The neutron diffraction pattern is shown in Fig. 1. Atomic positions and thermal parameters are listed in Table 1. Table 2 contains Ru–O bond distances, O–Ru–O and Ru–O–Ru bond angles.

The structure of $NaRu_2O_4$ is comprised of double chains of edge-sharing RuO_6 octahedra that then share corners with neighboring double chains, creating a zig-zag of RuO_6 dimers. Fig. 2 shows the structure of $NaRu_2O_4$, highlighting the pseudo-triangular channels created by the corner shared double chains where the alkali atom resides. The edge sharing between RuO_6 octahedra within the chain creates long chains along the c direction. Relatively short Ru–Ru distances are observed along the c-axis (~2.8 Å). Each double chain contains only one crystallographic type of Ru. The two distinct octahedral environments are shown in Fig. 3. The RuO_6 octahedra are mildly distorted: bond lengths range from 1.98 to 2.05 Å (average bond length 2.02 Å) and O–Ru–O angles within the octahedra span from 79° to 99°. Ru–O–Ru bond angles created by the

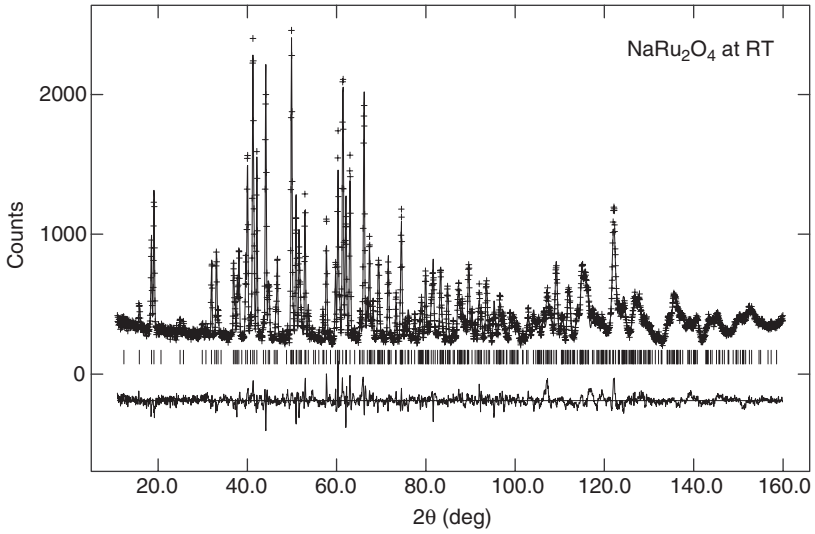

Fig. 1. Observed intensities (crosses) and calculated neutron diffraction pattern (solid line) for $NaRu_2O_4$ at 295 K. Vertical lines show reflection positions. Differences between the observed and the calculated intensities are shown at the bottom of the figure.

Table 1
Atomic positions and thermal parameters of $NaRu_2O_4$, s.g. *Pnma* (#62)

Atom	Site	x	y	z	U_i/U_e*100
Ru1	*4c*	0.0603(3)	1/4	0.1152(2)	1.00(7)
Ru2	*4c*	0.0848(3)	1/4	0.6036(2)	1.07(6)
Na1	*4c*	0.2399(6)	1/4	0.3397(5)	1.29(11)
O1	*4c*	0.2946(3)	1/4	0.6594(3)	0.76(8)
O2	*4c*	0.3847(3)	1/4	0.9751(3)	1.02(7)
O3	*4c*	0.4730(3)	1/4	0.2181(3)	0.66(8)
O4	*4c*	0.0870(3)	1/4	0.9347(3)	0.78(8)

$a = 9.2737(4)$ Å, $b = 2.8215(1)$ Å, $c = 11.1701(5)$ Å, $Z = 4$.

Table 2
Bond lengths and bond angles in $NaRu_2O_4$

	Bond length (Å)		Bond length (Å)
Ru1–O1 2	2.0110(28)	Na–O1 2	2.480(6)
Ru1–O3 1	2.031(4)	Na–O2 2	2.370(5)
Ru1–O4 2	2.0415(33)	Na–O3 1	2.553(6)
Ru1–O4 1	2.031(4)	Na–O3 1	2.558(6)
Ru2–O1 1	2.043(4)	Na–O4 2	2.386(5)
Ru2–O2 2	2.0314(33)		
Ru2–O2 1	2.053(4)		
Ru2–O3 2	1.9785(32)		
	Bond angle (°)		**Bond angle (°)**
O1–Ru1–O1	89.10(16)	O2–Ru2–O2	79.82(13)
O1–Ru1–O3	92.38(15)	O2–Ru2–O3	89.94(10)
O1–Ru1–O4	99.32(15)	O2–Ru2–O3	171.63(19)
O1–Ru1–O4	91.72(8)	O3–Ru2–O3	91.83(15)
O1–Ru1–O4	178.30(20)	O3–Ru2–O3	90.97(19)
O3–Ru1–O4	163.51(18)	Ru1–O1–Ru1	89.10(16)
O3–Ru1–O4	89.07(15)	Ru1–O4–Ru1	87.42(18)
O4–Ru1–O4	79.08(13)	Ru1–O4–Ru1	100.92(13)
O4–Ru1–O4	87.42(18)	Ru2–O2–Ru2	87.97(18)
O1–Ru2–O2	94.77(14)	Ru2–O2–Ru2	100.18(13)
O1–Ru2–O2	172.41(21)	Ru2–O3–Ru2	90.97(19)
O1–Ru2–O3	93.48(15)	Ru1–O1–Ru2	124.21(14)
O2–Ru2–O2	87.97(18)	Ru1–O3–Ru2	134.51(9)

shared edges within a double chain range from ~87° to 101°. The Ru–O–Ru bond angles created by shared corners of Ru1 and Ru2 octahedra measure 124° and 134.5°.

The structure of $Na_{3-x}Ru_4O_9$ was refined in the monoclinic space group $C2/m$ (#12) with lattice parameters of $a = 23.246(1)$ Å, $b = 2.8411(1)$ Å, $c = 11.0396(6)$ Å, and $\beta = 104.766(5)°$. The initial atomic positions were taken from the X-ray diffraction refinement on $Na_{3-x}Ru_4O_9$, reported by Darriet [12]. The neutron diffraction pattern for $Na_{3-x}Ru_4O_9$ is shown in Fig. 4. Trace amounts of RuO_2 are observed in the diffraction pattern, which explain the small features in the difference pattern. Atomic positions, site occupancies and thermal parameters are listed in Table 3. Except for the Na site occupation, the final results of the refinement are similar to those reported previously [12]. When refined as independent parameters, the occupancies for the Na1 and Na2 sites were found to be 1.10(4) and 1.05(5). As these are within three standard deviations of full occupancy, the sites were fixed at full occupancy in the final structural model. The Na3 site was found to clearly have a less than full occupancy, and its occupancy was refined independently in the final model. To decrease the effect of correlations among the thermal parameters for the Na atoms, they were constrained to be equal. The overall stoichiometry was therefore determined to be $Na_{2.7}Ru_4O_9$. The small difference between the starting and final Na content indicates, as is common in the preparation of alkali oxides, that excess Na was needed to prepare pure phase material. Unreacted alkali left the sample by volatilization. Table 4 contains Ru–O bond distances, O–Ru–O and Ru–O–Ru bond angles.

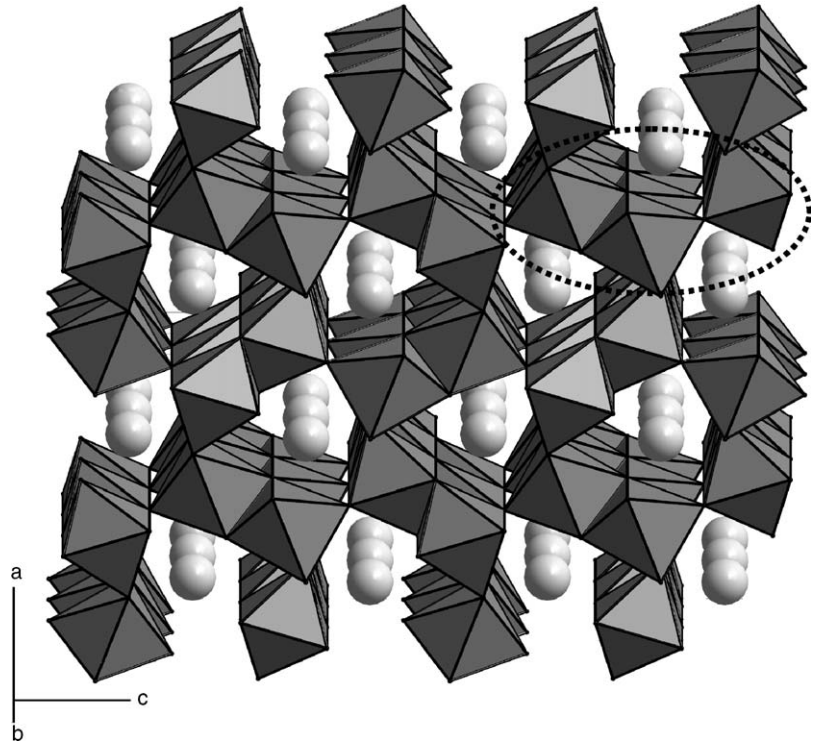

Fig. 2. The crystal structure of $NaRu_2O_4$. Na atoms are shown in light gray. The Ru atoms are in octahedral coordination with oxygen. The zig-zagging RuO_6 double chains create channels in which the alkali atoms reside. Double chains contain only one crystallographic type of Ru. The circled region is shown enlarged in Fig. 3.

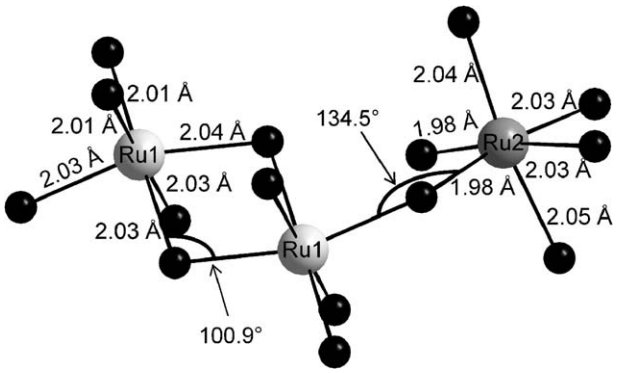

Fig. 3. The RuO_6 octahedral environment in $NaRu_2O_4$. The Ru atoms (Ru1 and Ru2) are shown as large gray spheres; oxygen atoms are smaller black spheres. The bond angle created by the corner sharing of $Ru(1)O_6$ and $Ru(2)O_6$ (= 134.5°) deviates significantly from the value of ~180° found in perovskites.

The structure of $Na_{2.7}Ru_4O_9$ can be related to that of $NaRu_2O_4$. However, in the case of $Na_{2.7}Ru_4O_9$, the corner-sharing chains are comprised of single, double or triple chains edge-shared RuO_6 octahedra (Fig. 5). This creates irregular zig-zags of RuO_6 octahedra as well as large cavities where multiple Na atoms reside. Structural refinement revealed non-stoichiometry on the Na sites caused by partial vacancy of the Na3 site.

The distinct RuO_6 octahedra are shown in Figs. 6a and b. Fig. 6a shows an edge-shared double chain (of Ru4's) connected through corner sharing to the neighboring Ru5 double chain. This is analogous to the octahedral environment seen in $NaRu_2O_4$. Still, the RuO_6 octahedra are distorted, with bond lengths ranging from 1.94 to 2.06 Å and O–Ru–O bond angles within the octahedra ranging from 81° to 95°.

Fig. 6b highlights the other octahedral environment in $Na_{2.7}Ru_4O_9$. The Ru2 and 2 Ru3 octahedra share edges (within the chains), while the Ru1 and Ru3 metal–oxygen octahedra share corners (between chains). This creates a motif of triple chains interspaced with single chains of RuO_6 octahedra.

Bond valence sums (BVS) were calculated for the Ru atoms in both compounds using the method described in Brese and O'Keeffe [17]. The results are shown in Table 5. The BVS for $NaRu_2O_4$ are close to the formal charge determined from the stoichiometry. (The bond valence sum of RuO_2 is 4.2 valence units, so lattice strain may be responsible for the deviation from the expected valence). For $Na_{2.7}Ru_4O_9$, the BVS vary from 3.5 to 4.0 valence units.

3.2. Magnetic susceptibility

Fig. 7 shows the χ vs. T plot for $NaRu_2O_4$ and $Na_{2.7}Ru_4O_9$. $NaRu_2O_4$ exhibits temperature independent paramagnetism, with a $\chi_0 = 1.2 \times 10^{-4}$ emu/mol$_{Ru}$ Oe. The slight upturn at low temperatures is most likely due to the presence of impurities. Curie–Weiss fitting of the low

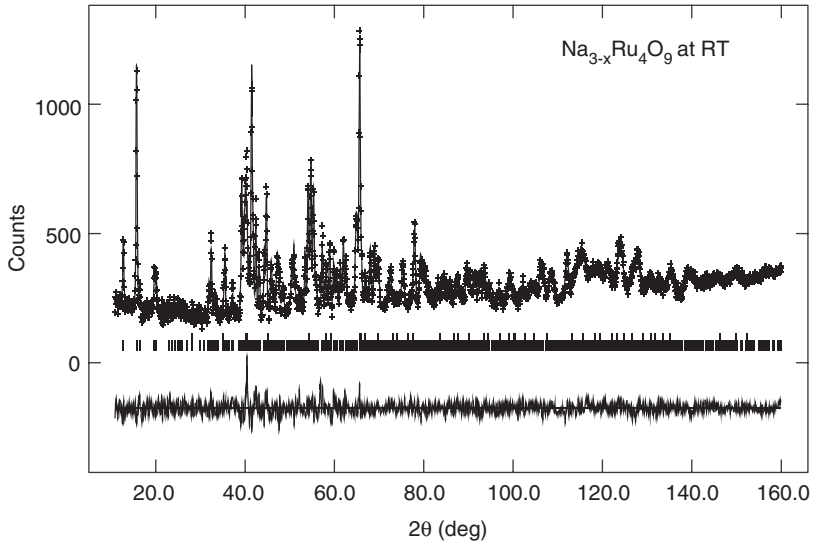

Fig. 4. Observed intensities (crosses) and calculated neutron diffraction pattern (solid line) for $Na_{2.7}Ru_4O_9$ at 295 K. Vertical lines show reflection positions. Differences between the observed and the calculated intensities are shown at the bottom of the figure.

Table 3
Atomic positions and thermal parameters of $Na_{2.7}Ru_4O_9$, s.g. $C2/m$ (#12)

Atom	Site	x	y	z	U_i/U_e*100	Occupancy
Ru1	*2a*	0	0	0	0.87(1)	1.00
Ru2	*2c*	0	0	1/2	0.87(1)	1.00
Ru3	*4i*	0.0591(3)	1/2	0.3097(7)	0.87(1)	1.00
Ru4	*4i*	0.2153(3)	1/2	0.3808(7)	0.87(1)	1.00
Ru5	*4i*	0.2720(3)	0	0.1299(6)	0.87(1)	1.00
Na1	*4i*	0.1388(9)	0	0.1026(17)	3.14(3)	1.00
Na2	*4i*	0.1456(8)	1/2	0.6055(15)	3.14(3)	1.00
Na3	*4i*	0.0730 (11)	0	0.8107(24)	3.14(3)	0.73(4)
O1	*4i*	−0.0600(4)	1/2	0.0113(8)	0.73(2)	1.00
O2	*4i*	0.0293(3)	0	0.1845(8)	0.62(2)	1.00
O3	*4i*	0.1339(4)	1/2	0.2788(8)	1.62(2)	1.00
O4	*4i*	0.0776(4)	0	0.4415(9)	1.29(2)	1.00
O5	*4i*	−0.0235(4)	1/2	0.3665(9)	1.56(3)	1.00
O6	*4i*	0.2015(4)	0	0.4959(8)	0.47(2)	1.00
O7	*4i*	0.2386(3)	0	0.2739(7)	0.24(2)	1.00
O8	*4i*	0.2114(4)	1/2	0.0436(9)	1.41(2)	1.00
O9	*4i*	0.3314(4)	1/2	0.2009(7)	0.44(2)	1.00

$a = 23.246(1)$ Å, $b = 2.8411(1)$ Å, $c = 11.0394(6)$ Å, $\beta = 104.766(5)^\circ$, $Z = 4$.

temperature inverse susceptibility data suggest that this upturn is caused by ~0.05% presence of spin 1 impurities, not visible in the neutron diffraction data. $Na_{2.7}Ru_4O_9$ is paramagnetic with $\chi_0 = 2 \times 10^{-4}$ emu/mol_{Ru} Oe. A linear fit from 125 to 200 K of the high temperature inverse susceptbility data, (inset, Fig. 7) showed Curie–Weiss behavior. The data yielded $\Theta_w = -11.8$ K, suggesting that the local moments in $Na_{2.7}Ru_4O_9$ are weakly antiferromagnetically coupled. The Curie constant was determined to be 0.0119 emu/mol Oe K, giving an effective moment of 0.309 μ_B per formula unit. This value is too large to be attributable to the presence of magnetic impurities. The anomalies observed by Cao et al. in the magnetic susceptibility of $Na_{3-x}Ru_4O_9$ were not observed in our samples [14].

3.3. Specific heat

The large χ_0 value observed in the magnetic susceptibility for $Na_{2.7}Ru_4O_9$ may indicate a large density of states at the Fermi level. Therefore, the specific heat of this compound was measured at low temperature. The data, shown in Fig. 8, show linear behavior above 7 K, with a small upturn at observed low temperatures. The electronic contribution to the specific heat (γ) was determined from the linear fit to be 15 mJ/mol_{Ru} K^2.

Table 4
Bond lengths and bond angles in $Na_{2.7}Ru_4O_9$

	Bond length (Å)		Bond length (Å)
Ru1–O1 4	2.017(6)	Na1–O1 2	2.405(17)
Ru1–O2 2	1.997(9)	Na1–O2 1	2.911(20)
Ru2–O4 2	2.064(10)	Na1–O7 1	2.592(20)
Ru2–O5 4	2.019(7)	Na1–O8 2	2.418(18)
Ru3–O2 2	1.980(9)	Na2–O4 2	2.518(15)
Ru3–O3 1	1.856(13)	Na2–O5 1	2.932(21)
Ru3–O4 2	2.000(9)	Na2–O6 2	2.444(14)
Ru3–O5 1	2.168(12)	Na2–O7 1	2.682(19)
Ru4–O3 1	1.939(12)	Na2–O9 2	2.508(15)
Ru4–O6 2	1.985(7)	Na3–O1 2	2.505(22)
Ru4–O6 1	2.061(11)	Na3–O2 1	2.393(27)
Ru4–O7 2	2.007(8)	Na3–O5 2	2.454(20)
Ru5–O7 1	1.939(11)	Na3–O9 1	2.256(26)
Ru5–O8 2	2.056(9)		
Ru5–O8 1	2.048(12)		
Ru5–O9 2	1.998(8)		
	Bond angle (°)		Bond angle (°)
O1–Ru1–O1	89.6(4)	O6–Ru4–O7	88.93(22)
O1–Ru1–O1	90.4(4)	O6–Ru4–O7	173.8(5)
O1–Ru1–O1	179.960(0)	O6–Ru4–O7	92.3(4)
O1–Ru1–O1	180.000(0)	O7–Ru4–O7	90.1(4)
O1–Ru1–O2	89.90(29)	O7–Ru5–O8	90.6(4)
O1–Ru1–O2	90.10(29)	O7–Ru5–O8	167.7(5)
O2–Ru1–O2	180.000(0)	O7–Ru5–O9	93.4(4)
O4–Ru2–O4	180.000(0)	O8–Ru5–O8	87.4(5)
O4–Ru2–O5	82.39(34)	O8–Ru5–O8	80.6(4)
O4–Ru2–O5	97.61(34)	O8–Ru5–O9	90.83(21)
O5–Ru2–O5	89.4(4)	O8–Ru5–O9	175.6(5)
O5–Ru2–O5	90.6(4)	O8–Ru5–O9	95.2(4)
O5–Ru2–O5	179.960(0)	O9–Ru5–O9	90.7(5)
O5–Ru2–O5	180.000(0)	Ru1–O1–Ru1	89.6(4)
O2–Ru3–O2	91.7(5)	Ru1–O2–Ru3	133.37(28)
O2–Ru3–O3	92.8(4)	Ru3–O2–Ru3	91.7(5)
O2–Ru3–O4	88.28(24)	Ru3–O3–Ru4	135.6(6)
O2–Ru3–O4	171.6(5)	Ru2–O4–Ru3	100.7(4)
O2–Ru3–O5	91.4(4)	Ru3–O4–Ru3	90.5(5)
O3–Ru3–O4	95.5(5)	Ru2–O5–Ru2	89.4(4)
O3–Ru3–O5	174.0(6)	Ru2–O5–Ru3	96.7(4)
O4–Ru3–O4	90.5(4)	Ru4–O6–Ru4	91.4(4)
O4–Ru3–O5	80.3(3)	Ru4–O6–Ru4	98.4(4)
O3–Ru4–O6	94.6(4)	Ru4–O7–Ru4	90.1(4)
O3–Ru4–O6	174.5(6)	Ru5–O7–Ru5	134.95(22)
O3–Ru4–O7	91.6(4)	Ru5–O8–Ru5	87.4(4)
O6–Ru4–O6	91.4(4)	Ru5–O8–Ru5	99.4(4)
O6–Ru4–O6	81.6(4)	Ru5–O9–Ru5	90.7(5)

4. Discussion

4.1. Structure

Both of the structures analyzed in this paper are built up from chains of edge sharing RuO_6 octahedra. The structural progression from RuO_2 to $Na_{2.7}Ru_4O_9$ is shown in Fig. 9. RuO_2 consists of single chains of edge shared RuO_6 octahedra. These chains share corners to create small square channels, which can be occupied by Li upon intercalation [18]. In the case of $NaRu_2O_4$, the chains are comprised of two RuO_6 octahedra, creating larger pseudo-triangular channels where the Na reside. In $Na_{2.7}Ru_4O_9$, the number of octahedra varies from one to three. The variation in chain length creates irregular channels large enough to accommodate three distinct Na sites. A similar progression is seen in the titanates. Chain lengths again vary from single octahedra (TiO_2), two edge-shared octahedra in $NaTi_2O_4$ [19] and a mixture of single, double and triple octahedral chains in $Na_2Ti_4O_9$ [20]. The titanates also exhibit structures built solely from triple chains ($Na_2Ti_6O_{13}$ [21] and $Na_2Ti_{12}O_{25}$ [22]) as well as chains of four-edge shared TiO_6 octahedra ($Na_2Ti_8O_{17}$ [23]). In this structural progression, the channels gradually increase in size. In $Cs_2Ti_5O_{11}$, the chain length is increased further to five-edge-shared octahedra [24]. However, the channels are open-ended forming a layered structure. We postulate that this structural progression may help to explain the properties in the sodium ruthenates, as described below.

The non-stoichiometry of $Na_{2.7}Ru_4O_9$ seems quite robust, since efforts to vary the Na content synthetically were not successful, suggesting it may be a line compound in the Na–Ru–O phase diagram. This can be possibly explained by the three different Na–O coordination polyhedra. In the case of Na1 and Na2, the Na is coordinated to eight oxygens, which is common for alkali ions. However, Na3 (the fractionally occupied site) is coordinated to only six oxygen. The lower stability of this coordination sphere could be responsible for the decreased occupancy. In addition, the overall size of the channel created by the metal octahedra may inhibit full occupancy of the site. The distance between Na1 and Na3 is only 3.19 Å, while the Na2–Na3 is much longer (3.47 Å). Therefore, Na–Na repulsion between Na1 and Na3 may play a role in making complete occupancy of Na3 unfavorable. Electronically, the fractional occupancy on the Na site may also help to stabilize the metal–oxygen framework of this compound. The reduction from full occupancy formally oxidizes the ruthenium atoms from $Ru^{3.75+}$ to $Ru^{3.83+}$, moving towards ruthenium's favored 4+ formal oxidation state.

The five distinct RuO_6 octahedra in $Na_{2.7}Ru_4O_9$ are of interest due to their distortion. In the single chain (comprised of $Ru(1)O_6$ octahedra), the degree of distortion is minimal, with a small contraction occurring along the '*z*-direction' of the polyhedra. A similar level of regularity is seen in the $Ru(2)O_6$ octahedron, with only a slight lengthening of the Ru–O bond along the '*z*-direction'. The double chains (comprised of Ru4 and Ru5) show an asymmetric distortion of the Ru–O bond lengths. However, it is the $Ru(3)O_6$ octahedron that displays the greatest degree of distortion, with extreme asymmetry in the Ru–O bond lengths along the *z*-direction, ranging from 1.86 to 2.18 Å. Curiously, the average bond length for all the octahedra (including $Ru(3)O_6$) is still chemically reasonable. The driving force for these distortions is unknown at the present time. In both compounds, the observed

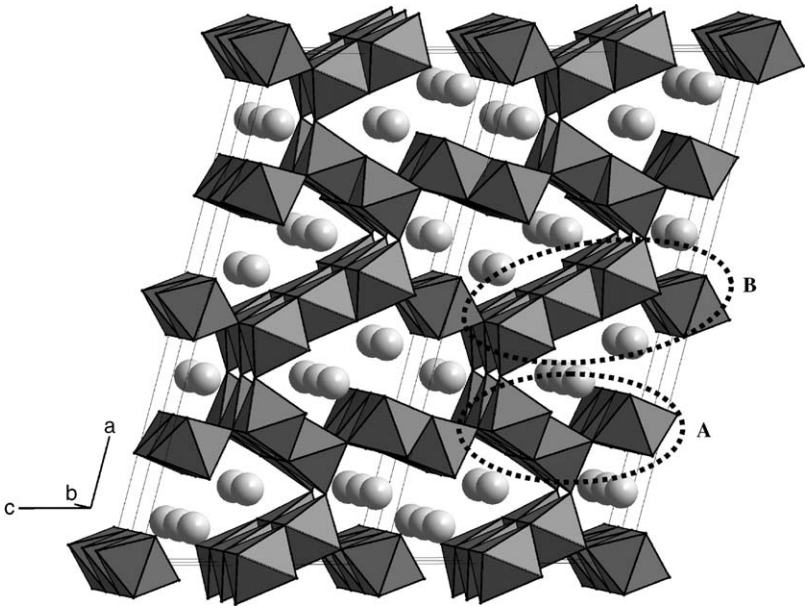

Fig. 5. The crystal structure of $Na_{2.7}Ru_4O_9$. Na atoms are shown in light gray. The Ru atoms are in octahedral coordination with oxygen which are located at the corners of the octahedra. The cavities created by the linking of the single, double and triple chains of RuO_6 octahedra are large enough to accommodate multiple Na ions. Circled regions are shown in greater detail in Fig. 6a and 6b.

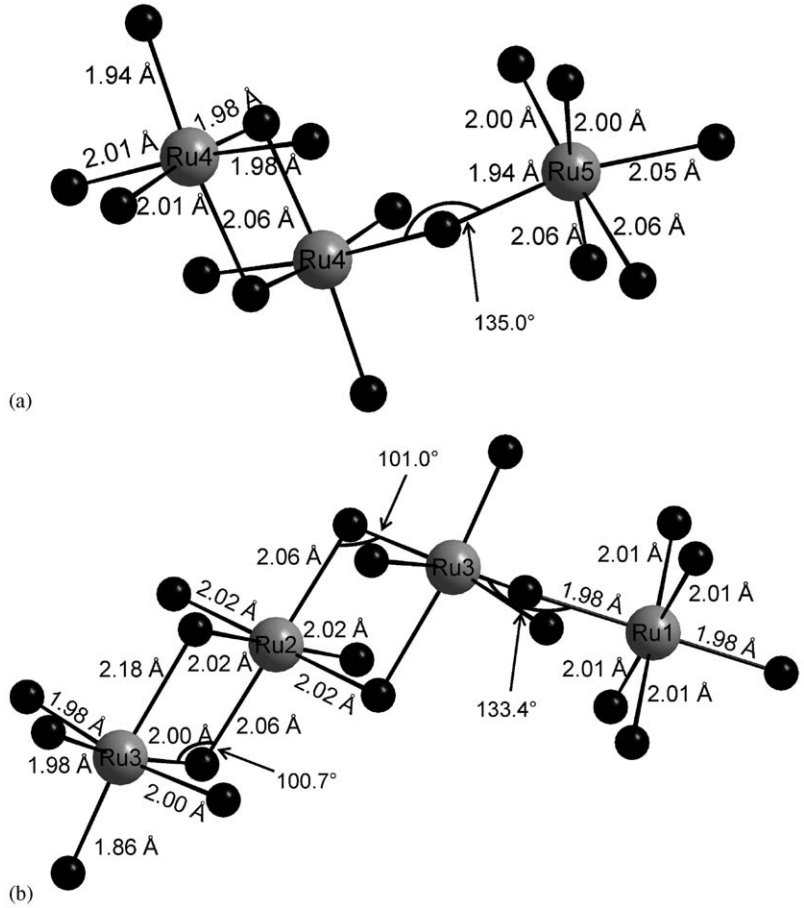

Fig. 6. The RuO_6 octahedral environments in $Na_{2.7}Ru_4O_9$. The Ru atoms are shown as large gray spheres; oxygen atoms are smaller black spheres: (a) RuO_6 octahedra are very similar to those seen in $NaRu_2O_4$. The Ru4–O–Ru5 angle is largely distorted from the expected 180°. (b) The RuO_6 octahedra within the triple chain are strongly distorted. O–Ru–O angles created by the edge sharing of Ru2 and Ru3 octahedra are widened to 101° (from 90°). The Ru3–O bond lengths along the z direction show extreme deviation from expected values.

O–Ru–O and Ru–O–Ru bond angles are similar to those present in the hollandites [25]. Deviations from the expected values for corner- or edge-shared octahedra can be attributed to lattice strain.

Lastly, there exists the possibility for metal–metal bonding in both of these compounds. Although most of the Ru–Ru distances are greater than 3 Å, shorter metal–metal distances are observed along one direction in the structure. Within the edge-shared double or triple chains of either compound, the Ru–Ru distances are approximately 3.1 Å. In $NaRu_2O_4$, the Ru1–Ru1 distance is 3.16 Å and the Ru2–Ru2 distance is 3.14 Å. In the triple chains of $Na_{2.7}Ru_4O_9$, the Ru3–Ru2 distance is 3.13 Å while the Ru–Ru distances for the Ru4 and Ru5 double chains are 3.05 and 3.14 Å, respectively. The distance separating the Ru atoms increases to ~3.6 Å for both compounds where the octahedra share corners, not edges. However, the distance between ruthenium atoms along the infinite chains in the *b* direction is ~2.8 Å in both $NaRu_2O_4$ and $Na_{2.7}Ru_4O_9$. Although the observed distance is somewhat longer than the distance generally taken as indicative of metal–metal bonding in the ruthenates (2.5 Å) [26,27], this shorter distance would give rise to enhanced metal–metal interactions along this crystallographic direction. Further studies on single crystals would be beneficial in determining whether such increased overlap dramatically influences the electronic or magnetic properties.

Table 5
Bond valence sums (BVS) for the different Ru sites in $NaRu_2O_4$ and $Na_{2.7}Ru_4O_9$

$NaRu_2O_4$		$Na_{2.7}Ru_4O_9$	
Formal valence on Ru: +3.5		Formal valence on Ru: +3.83	
Atom	BVS	Atom	BVS
Ru1	3.6	Ru1	3.8
Ru2	3.7	Ru2	3.5
		Ru3	4.0
		Ru4	3.9
		Ru5	3.7

4.2. Magnetism

Looking at the BVS for $Na_{2.7}Ru_4O_9$ allows us to speculate on the origin of the local moment magnetism observed in this compound. From the Curie–Weiss fit, the observed moment is 0.3 μ_B per Ru. It may be that the magnetic moment arises from the localization of electrons on one of the crystallographic Ru sites. When looking at the BVS for the ruthenium atoms, Ru2 and Ru3 are statistically different from the other three crystallographic sites, with valences of ~3.5 and 4, respectively. The lower bond valence sum on Ru2 could be indicative of Ru^{3+} (d^5, spin 1/2, ~1.8 μ_B). Given that Ru2 accounts for 1/8 of the total Ru atoms in the compound, the expected (spin only) magnetic moment if it is only coming from this site would be ~0.23 μ_B, close to the value observed. In RuO_2 and $NaRu_2O_4$, where only single or double chains exist, no localized magnetic moments are observed. The addition of triple chains to the structure may therefore give rise to the observed magnetic moment in $Na_{2.7}Ru_4O_9$. Alternatively, of course, the observed moment could be from itinerant electron magnetism.

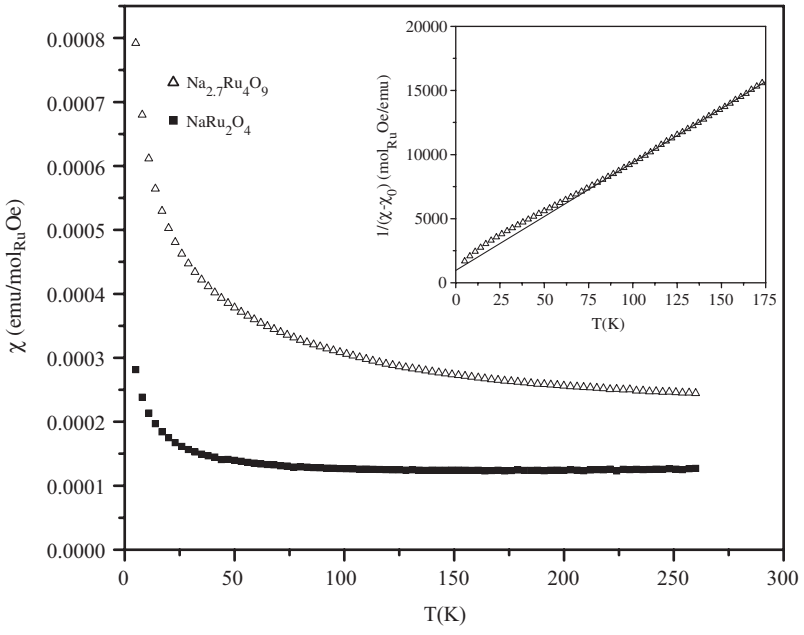

Fig. 7. Magnetic susceptibility vs. temperature data for $NaRu_2O_4$ (■) and $Na_{2.7}Ru_4O_9$ (△). $\chi_0 = 1.2 \times 10^{-4}$ emu/mol$_{Ru}$ Oe for $NaRu_2O_4$, $\chi_0 = 2.0 \times 10^{-4}$ emu/mol$_{Ru}$ Oe for $Na_{2.7}Ru_4O_9$. Inset: Inverse magnetic susceptibility vs. temperature data for $Na_{2.7}Ru_4O_9$. A linear fit of the high temperature data from 125 to 200 K shows Curie–Weiss behavior, giving $\Theta_{cw} = -11.8$ K and $C = 0.0119$ emu/mol Oe K.

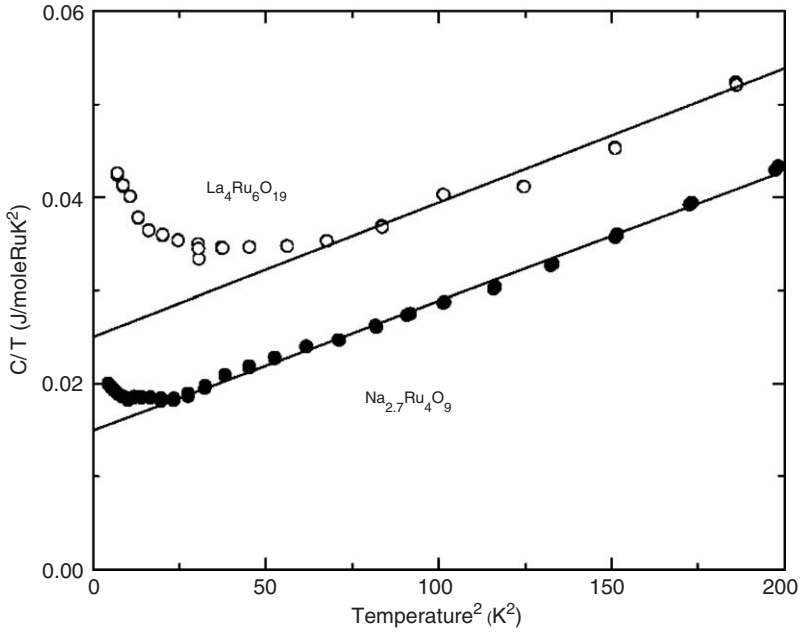

Fig. 8. Specific heat data vs. temperature data for $Na_{2.7}Ru_4O_9$ (●), plotted with $La_4Ru_6O_{19}$ (○) for reference. Linear fitting to the $Na_{2.7}Ru_4O_9$ data reveal an electronic contribution to the specific heat (γ) of 15 mJ/mol K^2.

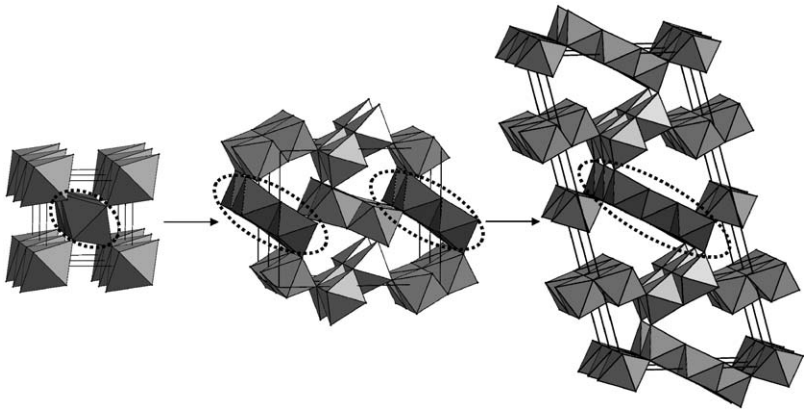

Fig. 9. The structures of RuO_2, $NaRu_2O_4$ and $Na_{2.7}Ru_4O_9$. The common structural motif (chains of edge sharing octahedra) is circled. The chains grow from one, to two, to three edge-shared octahedra in the three structures.

4.3. Specific heat

The low temperature specific heat data can be fit to $C = \gamma T + \beta T^3$, where the T^3 term is the low temperature contribution from the lattice, and the γ represents the electronic contribution, and can be used to determine the density of states at the Fermi level. Although the observed γ for $Na_{2.7}Ru_4O_9$ (= 15 mJ/mol$_{Ru}$ K^2) is much larger than the free electron value of 1 mJ/mol$_{Ru}$ K^2, it is not as large as some of the more interesting ruthenates: such as Sr_2RuO_4 (an exotic superconductor with $\gamma = 40$ mJ/mol$_{Ru}$ K^2 [28,29]) or $La_4Ru_6O_{19}$ (a material near a quantum critical point with $\gamma = 25$ mJ/mol$_{Ru}$ K^2 [30]). The γ value for $Na_{2.7}Ru_4O_9$ suggests that it may display some interesting transport or thermodynamic properties if studied in more detail. The specific heat data for $Na_{2.7}Ru_4O_9$ in Fig. 8 is plotted along with the specific heat data from $La_4Ru_6O_{19}$. Both compounds exhibit a small upturn at very low temperatures. In the case of $La_4Ru_6O_{19}$, this was attributed to the presence of magnetic fluctuations, which may be the case for $Na_{2.7}Ru_4O_9$, as well.

5. Conclusions

We have reported the crystal structure of two ruthenate bronzes, $NaRu_2O_4$ and $Na_{3-x}Ru_4O_9$, refined from powder neutron diffraction. Neutron data showed that $Na_{3-x}Ru_4O_9$ is a non-stoichiometric compound with $x = 0.3$. Magnetic data reveal temperature independent paramagnetism in $NaRu_2O_4$. $Na_{2.7}Ru_4O_9$ exhibits paramagnetism

with $\Theta_w = -11.8\,K$ and a Curie constant of $0.0119\,mol\,Oe/emuK$. Specific heat data reveal an enhanced contribution of the conduction electrons, with $\gamma = 15\,mJ/mol_{Ru}\,K^2$. Further work, including the growth of single crystals of both compounds, would be advantageous in exploration of possible anisotropy in the transport properties and the origin of the enhanced electronic contribution to the specific heat in $Na_{2.7}Ru_4O_9$.

Acknowledgment

The work at the Princeton University was supported by the National Science Foundation, Grant DMR-0244254.

References

[1] A. Callaghan, C.W. Moeller, R. Ward, Inorg. Chem. 5 (1966) 1572.
[2] J.T. Rijssenbeek, R. Jin, Y. Zadorozhny, Y. Liu, B. Batlogg, R.J. Cava, Phys. Rev. B 59 (1999) 4561–4564.
[3] Y. Maeno, H. Hashimoto, K. Yoshida, S. Nishizaki, T. Fujita, J.G. Bednorz, F. Lichtenberg, Nature 372 (1994) 532–534.
[4] M.T. Weller, R.W. Hughes, J. Rooke, C.S. Knee, J. Reading, Dalton Trans. (2004) 3032–3041.
[5] M.L. Foo, W.L. Lee, T. Siegrist, G. Lawes, A.P. Ramirez, N.P. Ong, R.J. Cava, Mater. Res. Bull. 39 (2004) 1663–1670.
[6] Z.Q. Mao, T. He, M.M. Rosario, K.D. Nelson, D. Okuno, B. Ueland, I.G. Deac, P. Schiffer, Y. Liu, R.J. Cava, Phys. Rev. Lett. 90 (2003).
[7] I.S. Shaplygin, V.B. Lazarev, Zh. Neorg. Khim. 25 (1980) 3355–3361.
[8] M. Shikano, R.K. Kremer, M. Ahrens, H.J. Koo, M.H. Whangbo, J. Darriet, Inorg. Chem. 43 (2004) 5–7.
[9] M. Shikano, C. Delmas, J. Darriet, Inorg. Chem. 43 (2004) 1214–1216.
[10] K. Takada, H. Sakurai, E. Takayama-Muromachi, F. Izumi, R.A. Dilanian, T. Sasaki, Adv. Mater. 16 (2004) 1901–1905.
[11] J. Darriet, A. Vidal, Bull. Soc. Fr. Mineral. Cristallogr. 98 (1975) 374–377.
[12] J. Darriet, Acta Crystallogr. Sect. B B30 (1974) 1459–1462.
[13] Y. Onoda, S.H. Chung, A. Watanabe, T. Mitsuhashi, Solid State Ion. 136 (2000) 365–370.
[14] G. Cao, S. McCall, F. Freibert, M. Shepard, P. Henning, J.E. Crow, Phys. Rev. B53 (1996) 12215–12219.
[15] K. Yamaura, Q. Huang, M. Moldovan, D.P. Young, A. Sato, Y. Baba, T. Nagai, Y. Matsui, E. Takayama-Muromachi, Chem. Mater. 17 (2005) 359–365.
[16] A. Larson, R.B. Von Dreele, Los Alamos National Laboratory, 1994.
[17] N.E. Brese, M. O'Keeffe, Acta Crystallogr. Sect. B 47 (1991) 192–197.
[18] P. Dalard, D. Deroo, D. Foscallo, C. Mouliom, Solid State Ion. 15 (1985) 91–94.
[19] J. Akimoto, H. Takei, J. Solid State Chem. 79 (1989) 212–217.
[20] J. Akimoto, H. Takei, J. Solid State Chem. 83 (1989) 132–139.
[21] S. Andersson, A.D. Wadsley, Acta Crystallogr. 15 (1962) 194–201.
[22] K.J. Range, H. Fischer, F. Ketterl, S. Afr. J. Chem. 40 (1987) 233–236.
[23] A.D. Wadsley, W.G. Mumme, Acta Crystallogr. Sect. B B24 (1968) 392–396.
[24] J. Kwiatkowska, I.E. Grey, I.C. Madsen, L.A. Bursill, Acta Crystallogr. Sect. B 43 (1987) 258–265.
[25] M. Wilhelm, R. Hoppe, Z. Anorg. Allg. Chem. 438 (1978) 90–96.
[26] P. Khalifah, R.J. Cava, Phys. Rev. B 6408 (2001) art. no.-085111.
[27] F. Abraham, J. Trehoux, D. Thomas, Mater. Res. Bull. 12 (1977) 43–51.
[28] S. Nishizaki, Y. Maeno, S. Farner, S. Ikeda, T. Fujita, Physica C 282 (1997) 1413–1414.
[29] Y. Maeno, Physica C 282 (1997) 206–209.
[30] K. Tsuchida, C. Kato, T. Fujita, Y. Kobayashi, M. Sato, J. Phys. Soc. Jpn. 73 (2004) 698–702.